

# Self-organized pattern formation in laser-induced multiphoton ionization

Robert Buschlinger,<sup>1</sup> Stefan Nolte,<sup>2,3</sup> and Ulf Peschel<sup>1</sup>

<sup>1</sup>*Institute of Optics, Information and Photonics,  
University of Erlangen-Nürnberg, 91058 Erlangen, Germany*

<sup>2</sup>*Institute of Applied Physics, Abbe Center of Photonics,  
Friedrich-Schiller-Universität Jena, 07743 Jena, Germany*

<sup>3</sup>*Fraunhofer Institute for Applied Optics and Precision Engineering, 07745 Jena, Germany*

We use finite-difference time-domain modelling to investigate plasma generation induced by multiphoton absorption of intense laser light in dielectrics with tiny inhomogeneities. Plasma generation is found to be strongly amplified around nanometer-sized inhomogeneities as present in glasses. Each inhomogeneity acts as the seed of a plasma structure growing against the direction of light propagation. Plasma structures originating from randomly distributed inhomogeneities are found to interact strongly and to organize in regularly spaced planes oriented perpendicularly to the laser polarization. We discuss similarities between our results and nanogratings in fused silica written by laser beams with spatially homogeneous as well as radial and azimuthal polarization.

Many dielectrics as e.g. silica glasses are known to be transparent within a wide frequency range. Only at high intensities absorption becomes possible, as electrons are promoted to the conduction band by nonlinear ionization processes.<sup>1</sup> The strong intensity dependence of multiphoton ionization allows for the selective excitation and laser-induced modification of a small focal region situated inside a material volume. Different kinds of material modification have been observed, including refractive index changes,<sup>2</sup> void formation<sup>3</sup> and subwavelength volume grating formation.<sup>4-6</sup>

Previous modelling efforts concerning laser energy deposition in dielectrics have concentrated on the temporal and spatial evolution of the laser pulse itself, while treating the material as homogeneous.<sup>7-10</sup> As far as nonlinear self-organization is concerned, a certain seed is required to start the process. Therefore, we follow a different approach and investigate the interaction of laser light with nanometer-sized inhomogeneities. This is of fundamental interest due to the inherent inhomogeneity of amorphous materials like silica glasses.<sup>11</sup> Such inhomogeneities have also been suggested to play a major role in volume nanograting formation.<sup>12</sup>

Our simulations are based on the standard parameters which can be found in the literature. A good overview of the parameters of laser light and free carriers present during nanograting formation has been given by Bulgakova et al.<sup>9</sup> There, the intensities achieved by focussing and nonlinear propagation inside the homogeneous material cause smooth, submetallic carrier density distributions. We use similar parameters, but in our case material inhomogeneities increase the local intensity and cause the formation of plasma spots. We demonstrate, that the ionization process is independent of the exact shape and nature of the initial inhomogeneities. However we can identify two regimes depending on the local carrier densities that are reached during irradiation. For low carrier densities, ionization enhancement remains confined to the initial region of field enhancement close to an inhomogeneity. For higher carrier densities, a single nanoplasma forming at an inhomogeneity site enhances further ion-

ization in its vicinity and acts as a seed for the growth of an extended structure. This regime of strong interaction is similar to the ionization instability which has been predicted for tunneling ionization in gasses<sup>13,14</sup> and which has been suggested to play a similar role in the ionization of transparent dielectrics.<sup>9</sup> In both cases, intricate structures with high carrier densities can be formed. However, the local field enhancement around an existing nanoplasma plays a much more important role in our case.

We further examine optical self-organization in material systems with randomly distributed nanometer-sized inhomogeneities. We observe the formation of planar structures aligned perpendicularly to the laser polarization with a self-organized period related to the laser wavelength. We discuss the similarities to experimentally observed nanograting damage patterns and the possible connection of our results to these phenomena.

## I. NUMERICAL MODEL

For our model, we use a nonlinear finite-difference time-domain (FDTD) approach, which previously has been applied to the modelling of ionization and void formation in silica.<sup>10,15</sup> Maxwell's equations

$$\begin{aligned}\frac{\partial \vec{D}}{\partial t} &= \frac{1}{\mu_0} \nabla \times \vec{B} - \vec{J} \\ \frac{\partial \vec{B}}{\partial t} &= -\nabla \times \vec{E}\end{aligned}\quad (1)$$

with  $\vec{D} = \epsilon \vec{E} + \vec{P}$  are solved using the standard FDTD algorithm.<sup>16,17</sup> The response of the unexcited medium, which is dominated by valence band electrons, is included in the background permittivity  $\epsilon = n^2 \epsilon_0$ , using a linear refractive index  $n = 1.45$ .

We also incorporate the Kerr effect using the third-order material polarization  $\vec{P} = \epsilon_0 \chi_3 E^2 \vec{E}$ . This formulation assumes a scalar third order susceptibility  $\chi_3 =$

$2 \times 10^{-22} m^2 V^{-2}$ ,<sup>18</sup> which is a good approximation for linearly polarized light propagating in glass.

The remaining contributions to the material response are included via the current density  $\vec{J} = \vec{J}_d + \vec{J}_{mpi}$ , where the ionization current  $\vec{J}_{mpi}$  is used to model the energy loss of the electric field due to multiphoton ionization, which excites electrons to the conduction band.  $\vec{J}_d$  describes the optical response of these newly generated conduction band electrons based on a Drude model

$$\frac{\partial \vec{J}_d}{\partial t} = -\nu_e \vec{J}_d + \frac{e^2}{m_e} \rho \vec{E}. \quad (2)$$

In a complete model, the electron collision frequency  $\nu_e$  would have to be assumed to depend on carrier density and temperature. As a simplification, we assume it to have a constant value  $\nu_e = 10^{14} s^{-1}$  lying in the range of reported values.<sup>9,19,20</sup> As long as the resonant field-enhancement close to a nanoplasma is not completely damped by collisions, final results have turned out to be mostly independent of  $\nu_e$ .

The time dependent conduction band carrier density  $\rho$  is described with a rate equation taking into account multiphoton ionization and recombination

$$\frac{\partial \rho}{\partial t} = (\rho_0 - \rho) \nu_{mpi} - \frac{\rho}{\tau_{rec}}. \quad (3)$$

In this model, the free carrier density reaches saturation at a value of  $\rho_0 = 2 \times 10^{28} m^{-3}$ .<sup>15</sup> The electron recombination time is  $\tau_{rec} = 150 \times 10^{-15} s$ .<sup>21</sup> For an excitation wavelength of  $\lambda = 800 nm$  and a fused silica target with a band gap of  $W_{ion} = 9 eV$ , 6 photons are needed to promote an electron to the conduction band, resulting in an ionization rate

$$\nu_{mpi} = \frac{\sigma_6 I^6}{\rho_0} \quad (4)$$

with a cross-section of  $\sigma_6 = 2 \times 10^{-65} m^9 W^{-6} s^{-1}$ .<sup>18</sup> An expression for  $\vec{J}_{mpi}$  can be derived by equating the energy gain of electrons  $\frac{\partial}{\partial t} W = W_{ion} \nu_{mpi} (\rho_0 - \rho)$  due to multiphoton ionization to the energy loss of the electric field  $\vec{J}_{mpi} \vec{E}$ , yielding

$$\vec{J}_{mpi} = \frac{\sigma_6}{\rho_0} W_{ion} I^5 \vec{E} (\rho_0 - \rho). \quad (5)$$

The nonlinear equations that describe the electric field, ionization loss and carrier density are solved using a fixed-point iteration method at each FDTD-timestep.

Additional attention has to be paid to the modelling of inhomogeneities. As glass is an amorphous solid, nano-size inhomogeneities are always present due to local variations in the chemical structure<sup>22</sup> and to actual voids or gas inclusions.<sup>11,23</sup> It has also been reported, that material nonlinearities can be enhanced by a history of previous laser-irradiation.<sup>22,24,25</sup> Such effects could lead to an additional inhomogeneity in the nonlinear response. According to literature, voids in conventional silica take

up a fraction of 3% of the material volume<sup>11</sup> and have an average size of  $d = 0.6 nm$ ,<sup>23</sup> resulting in a mean spacing below  $20 nm$ . Such voids should be an appropriate model for a typical inhomogeneity. As will be shown in section II, ionization around a void leads to the same final plasma structure as ionization around a region with an enhanced ionization cross-section. Additionally, final results do not depend on the actual shape of the inhomogeneity, as long as the initial size does not exceed a few nanometers. This is to be expected, since scattering from small objects is dominated by the dipole mode and does not depend on the specific shape.<sup>26</sup> This means that once initial results are established with a fine discretization ( $\Delta x = 0.5 nm$ ) and realistic inhomogeneities, we can safely use comparatively large seed inhomogeneities and coarse discretizations. Nevertheless, to properly resolve the inhomogeneities and the induced plasma structures, the resolution should not exceed  $\Delta x = 5 nm$ . As the simulation of multiple laser pulses and the subsequent material modifications are outside the reach of present computational resources, we limit our scope to continuous illumination in order to understand the potential of purely optical self-organization processes. This approach can be viewed both as a limiting case of single-pulse excitation and as an extrapolation of the excitation with multiple pulses.

In all presented cases, the simulation volume is situated deep inside the bulk of the material. At the material boundaries far away from the focal region of the laser, intensities are considerably lower. We will start out with simple geometries where the exciting field is approximated as a plane wave and then proceed to more realistic simulations with focussed sources. The simulation volume is terminated by perfectly matched layers<sup>17</sup> in propagation direction. In transverse direction, we choose periodic boundary conditions. Initially, the material is taken to be unexcited and the conduction band carrier density is set to  $\rho = 0$ .

## II. SIMULATION RESULTS

Our simulations focus on the interaction of intense laser-light with materials with randomly distributed nanometer-sized inhomogeneities. To get a feeling for the basic processes, we start with a very simplified, but quasi-analytical model. We consider a spherical subwavelength inhomogeneity, in which plasma generation can occur due to a non-vanishing ionization cross-section. Plasma generated inside the sphere according to Eq. 3 causes a decrease of the dielectric constant according to Eq. 2. In the case of a sphere much smaller than the exciting wavelength, the fields can be calculated in a quasi-static approximation<sup>26,27</sup> (Figs. 1(a),(b)). Combined with envelope approximations of Eqs. 2 and 3, this model can also serve to estimate the temporal evolution of the carrier density and electric field strength inside the sphere (Fig. 1(c)). According to the electrostatic approxima-

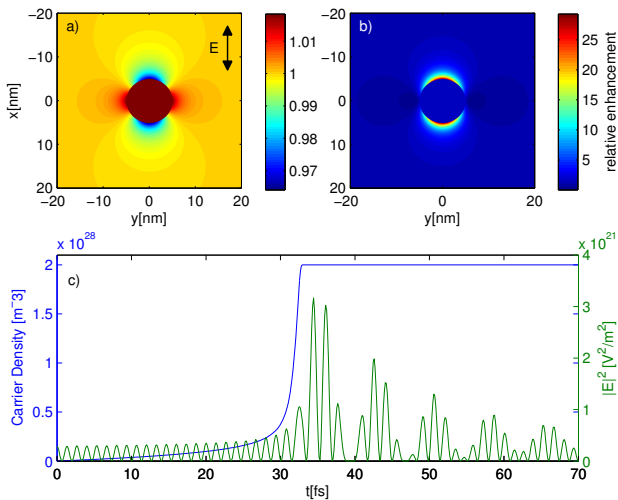


Figure 1: (color online). Scattering on a small inhomogeneity. a) and b): Local intensity enhancement for plasma spheres with different carrier densities  $\rho$  (to illustrate the field structure, calculations are done using the electrostatic approximation. Refractive indices are obtained from the Drude model). (a)  $\rho = 10^{26} m^{-3} \ll \rho_{Mie}$ . b)  $\rho = 2 \times 10^{28} m^{-3} > \rho_{Mie}$ . c): Temporal evolution of the carrier density and electric field in a small ionizable sphere in glass irradiated with a plane wave (amplitude  $E_0 = 1.7 \times 10^{10} Vm^{-1}$ ).

tion, a dipole wave is excited at the inhomogeneity site and interferes with the incident plane wave. Intensity is enhanced both inside the sphere and at its equator perpendicular to the incident electric field vector (Fig. 1(a)). The free electron density inside the sphere increases due to the positive feedback between the local electric field and the plasma refractive index (Fig. 1(c)). Eventually, the plasma reaches a carrier density where the dipole-resonance of the sphere comes close to the excitation frequency ( $\epsilon_{plasma}(\rho_{Mie}, \omega_{source}) = -2\epsilon_{background}$ ). At this point, carrier densities increase almost exponentially. The scattered field is now strongly enhanced and solely determines the nearfield intensity pattern. Due to the strong field enhancement, ionization continues even up to the maximum carrier density  $\rho = \rho_0$ , where saturation sets in. Pronounced intensity maxima now lie at the poles of the nanoplasma (Fig. 1(b)).

If ionization in the surrounding medium is taken into account, this field enhancement leads to the formation of an ionized region growing into the direction of the electric field. Since scattering is now mostly caused by the induced nanoplasma, the final structure is invariant concerning the microscopic details like shape, size and chemical nature of the seed inhomogeneity. Even if the initial inhomogeneity is a void instead of a region with an enhanced nonlinearity, field enhancement around the void leads to an amplified plasma generation, resulting in a similar evolution if a certain threshold is exceeded. To verify these guesses, we turn our attention to the complete FDTD-based model as described in section I.

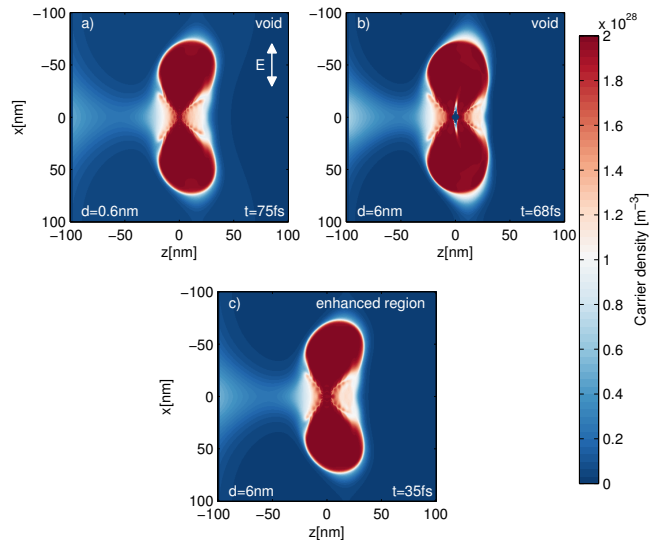


Figure 2: (color online). Carrier density (2D FDTD) for early stages of ionization around spherical voids ( $\sigma_{6,inh} = 0$ ,  $n = 1.0$ ) with different sizes as indicated in the figure as well as a region with an enhanced ionization cross-section  $\sigma_{6,inh} = \sigma_6 \times 5$ . Illumination is a continuous plane wave with amplitude  $E_0 = 1.7 \times 10^{10} Vm^{-1}$  normally incident from the left in all three cases.

We initially restrict simulations to a two-dimensional geometry, since this has shown to illustrate the growth process more clearly than the full three-dimensional case. For our later simulations we will return to three-dimensional geometries and show that the plasma structures growing in random media tend to reproduce the features seen in a 2D simulation.

We consider regions with an enhanced ionization cross-section  $\sigma_6$  (Figs. 2(c), 4), being conceptually close to the analytical model, as well as nanovoids with a diameter  $d = 0.6nm$  as present in silica and with a diameter increased by a factor of 10 (Figs. 2, 3). The results in Fig. 2 have been produced with a spatial resolution of  $\Delta x = 0.5nm$ . For the larger simulation volumes in Figs. 3 and 4, a much coarser resolution of  $\Delta x = 5nm$  has been used.

We find, that all three inhomogeneity models reproduce the initial predictions of the analytical model and lead to an almost exponential growth of identical plasma structures into polarization direction (Fig. 2(a)). Additionally we observe, that the results do not differ significantly if a coarser discretization is used. We conclude, that the final plasma structure is indeed invariant concerning the seed. However, the irradiation time or intensity needed to initiate the quasi-exponential growth depends on the nature and strength of the inhomogeneity. Based on Fig. 1(c) we can say, that growth is initiated if a carrier density of approximately half the resonant density is reached locally. For  $\lambda = 800nm$  and  $n = 1.45$  this corresponds to a value of  $\frac{\rho_{Mie}}{2} \approx 5 \times 10^{27} m^{-3}$ .

Growth in polarization direction only slows down as

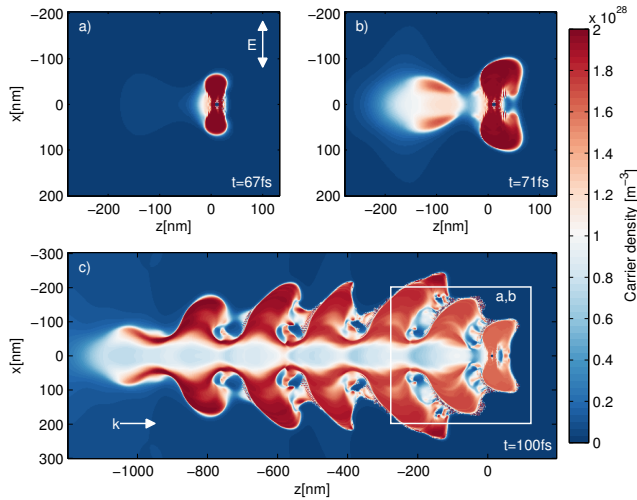


Figure 3: (color online). Plasma density (2D FDTD) around a single void ( $\sigma_{6,inh} = 0$ ,  $n = 1.0$ ,  $d = 7nm$ ) at the coordinate origin for several stages of structure growth. a) Plasma growth into the polarization direction. b) Saturation of growth and initiation of a second structure. c) Periodic plasma structure formed by subsequent growth. Illumination is a cw plane wave with amplitude  $E_0 = 1.7 \times 10^{10} Vm^{-1}$  incident from the left.

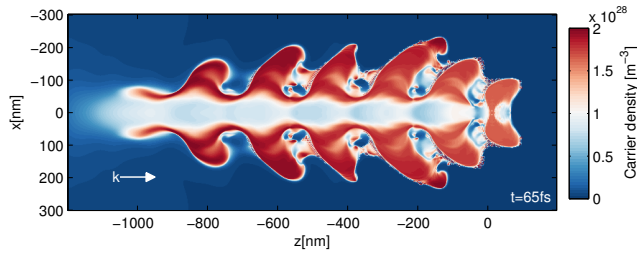


Figure 4: (color online). Plasma density (2D FDTD) around a single inhomogeneity with an enhanced ionization cross-section ( $\sigma_{6,inh} = \sigma_6 \times 15$ ,  $d = 7nm$ ) at the coordinate origin. Illumination is a cw plane wave with amplitude  $E_0 = 1.7 \times 10^{10} Vm^{-1}$  incident from the left.

the resulting structure leaves the sub-wavelength domain. Now the plasma acts as a nanoantenna whose maximum reflectivity would be reached at a size of  $\frac{\lambda}{2n}$ . However, there is strong back-reflection already at smaller sizes. Due to constructive interference with the incident wave, further ionization is stimulated along the negative propagation direction (Fig. 3(b)) and a new structure is formed in front of the old one. At this point, the lateral growth of the initial structure is inhibited, leading to a finite size in polarization direction.

During few optical cycles, a new structure is formed at the intensity maximum caused by reflection from the previous one. In this way, a periodic plasma chain with wavelength dimensions is initiated by a tiny seed inhomogeneity of almost arbitrary nature (compare Figs. 3(c) and 4) and grows backwards against the propagation direction.

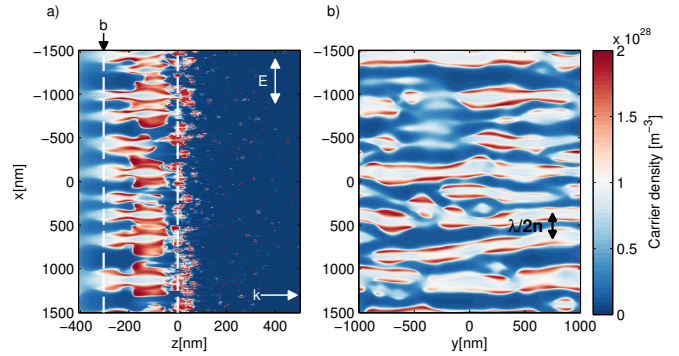


Figure 5: (color online). Carrier density generated by a plane wave (amplitude  $E_0 = 1.7 \times 10^{10} Vm^{-1}$ ) normally incident on a half space ( $z > 0$ ) filled with inhomogeneities ( $p_{inh} = 0.01$ ,  $\sigma_{6,inh} = 60\sigma_6$ ). Structures grow backward from the inhomogeneous/homogeneous border at  $z = 0$  and form a grating with a period of  $\sim \frac{\lambda}{2n} = 275nm$ . Polarization and laser propagation direction are indicated in panel a). Panel b) shows a cut through the grating planes at  $z = -300nm$ .

We now turn to the study of randomly distributed inhomogeneities in a three-dimensional volume. In all the simulations presented here, we place pixel-sized inhomogeneities with a density  $p_{inh}$  and leave the background medium unperturbed. As expected we again observe structure growth starting from the individual seed inhomogeneities. For nanovoids or regions with a weakly enhanced ionization cross-section as described above, the structures are sparsely distributed throughout the material volume and do not interact. However for higher densities, a large number of plasma structures competes in the growth process, resulting in an onset of self-organization. To explore such effects, we now allow for stronger ionization-enhancement inside the inhomogeneities (Figs. 5-8).

In such systems, we observe the dense growth of the structures we already described for the two-dimensional case. During their backwards directed growth, the structures also expand into the third direction not covered by our previous two-dimensional simulations. They do so until they merge with their neighbours to form extended plasma planes oriented perpendicularly to the polarization direction. Due to destructive interference of scattered and incident light, ionization is suppressed directly adjacent to each plasma plane and enhanced at a distance of approximately  $\frac{\lambda}{n}$ . We note, that the field suppression and enhancement pattern in polarization direction around a single complex plasma structure is still similar to the one for a small plasma sphere despite the differences in shape and size.

This effect leads to an interaction between separate structures. As a result, order emerges during growth and a periodic pattern can be formed. Since many structures form simultaneously and interaction only becomes relevant during the growth process, the resulting period is not completely determined by the position of the inten-

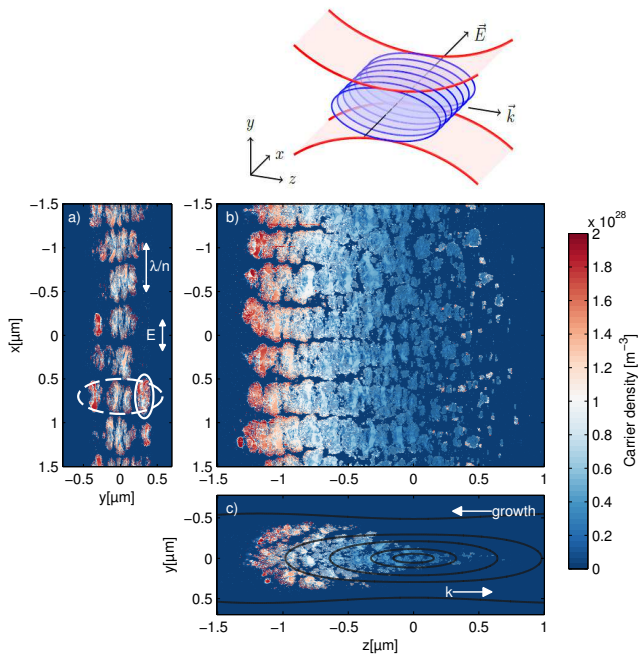


Figure 6: (color online). Carrier density within an inhomogeneous volume ( $p_{inh} = 0.01$ ,  $\sigma_{6,inh} = 40 \times \sigma_6$ ) illuminated with a beam (maximum field strength in the homogeneous case  $E_0 = 1.9 \times 10^{10} \text{Vm}^{-1}$ ,  $NA = 0.8$ ) focussed in  $y$ -direction, polarized in  $x$ -direction and propagating in  $z$ -direction. The linear focus is located at  $z = 0$  (see overlay of lines of equal field strength  $|E|^2$  in panel c)). The sketch shows the focussing geometry and orientation of periodic structures.

sity maximum, but also depends on growth conditions like the density and ionization cross section of seed inhomogeneities or the intensity of the excitation.

The smallest period can be observed under plane wave illumination. In this case, structures closest to the source plane tend to grow first and scatter light backwards, thus preventing any growth inside the simulation volume behind them. To observe the free growth and competition between different structures, we only fill a subspace with inhomogeneities, leaving the space close to the source unperturbed. Plasma structures form mainly at the border of the inhomogeneous region and grow backwards into the unperturbed region, where intensity is high (Fig. 5). Now only strong suppression close to the individual structures inhibits the growth of their neighbours, resulting in a period as small as  $\frac{\lambda}{2n}$ . Note that although growth starts at an interface, the resulting structure formation remains a volume effect which can only to a certain extent be compared to surface grating formation, which has been explained in terms of interference of dipole radiation initiated at a rough material surface.<sup>28,29</sup> In our case, the self-organized period is caused by the growth of densely arranged metallic plasma structures initiated at the inhomogeneities on the interface.

In more realistic simulations, we fill the entire simulation volume with inhomogeneities and use focussed

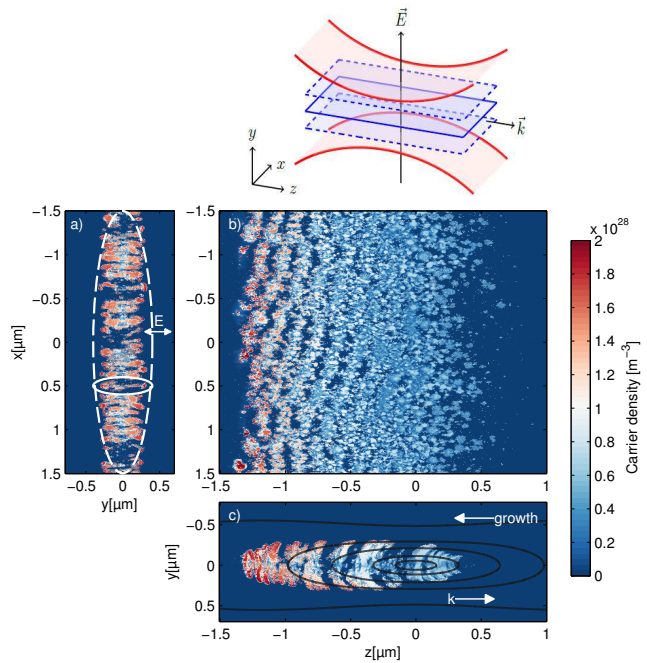


Figure 7: (color online). Carrier density within an inhomogeneous volume ( $p_{inh} = 0.01$ ,  $\sigma_{6,inh} = 40 \times \sigma_6$ ) illuminated with a beam (maximum field strength in the homogeneous case  $E_0 = 1.9 \times 10^{10} \text{Vm}^{-1}$ ,  $NA = 0.8$ ) focussed and polarized in  $y$ -direction, and propagating in  $z$ -direction. The linear focus is located at  $z = 0$  (see overlay of lines of equal field strength  $|E|^2$  in panel c)). The sketch shows the focussing geometry and orientation of ionization structures.

sources to control the location of initial structure growth. First we use a source polarized in  $x$ -direction and focussed only in  $y$ -direction, with  $z$  being the propagation direction (see Fig. 6). In  $x$ -direction the source profile has an infinite size to allow for the formation of many grating planes. In  $y$ -direction the beam is assumed to have a gaussian shape. As expected, structures first emerge in the focal volume and grow backwards over micrometer distances into regions of decreasing intensity (Fig. 6). Self-organization in this case is dominated by mutual enhancement and we observe periods around  $\frac{\lambda}{n}$ . Since the planes form inside an initially disordered volume, self-organization only starts after a certain distance of backwards growth outside the original focus. As can be seen in Fig. 6(c), the transverse size of the ionized region increases at the distance where self-organization sets in (approximately  $500 \text{nm}$  behind the original focus), leading to a “carrot-shaped” growth. We observe, that the individual grating planes, as highlighted with a dashed ellipse in Fig. 6(a)), consist of several smaller structures, as highlighted with a second ellipse, having a finite size below  $\frac{\lambda}{2n}$  in polarization direction. These correspond to the original wing-structure as it was observed in Fig. 3(a). Similiar to the case of Fig. 5, the individual structures tend to merge in the direction perpendicular to the polarization. However due to the random distribution of

seed inhomogeneities, the emerging structures are not as regular as the ones observed previously.

To further demonstrate the effect of polarization, we continue using the beam geometry of Fig. 6, but choose an excitation polarized in  $y$ -direction (Fig. 7). In this case, one would expect the grating planes to be extended along the  $x$ - and  $z$ - directions and arranged periodically along the  $y$ -direction. Since the exciting beam has a limited size in  $y$ -direction, we only observe a single structure, corresponding to a single grating plane (Fig. 7 (c)). As one would expect, no periodicity in  $x$ -direction can be found (Fig. 7(a)). However, similar to Fig.6(a), the grating plane consists of smaller structures, which have grown from seed inhomogeneities and which have partly merged in  $x$ -direction. As suggested by the plasma structures in Figs. 3(c) and 4, we also observe some periodicity along the propagation direction (Fig. 7 (b)).

We further consider spatially localized radially and azimuthally polarized beams. Again we observe the formation of plasma planes perpendicular to the local polarization. For an azimuthally polarized beam, this leads to a star-shaped pattern containing several planes (Fig. 8(a),(b)). In the radially polarized case, we obtain a single ring structure caused by the transverse field components and a small structure in the beam center caused by the maximum of the longitudinal component (Fig. 8(c),(d)). Again, the individual planes in the star-shaped pattern in Figs.8(a),(b) and the single ring structure in Figs.8(c),(d) are made up of smaller structures which tend to merge in the directions perpendicular to the exciting polarization. In general the plasma planes generated by radially polarized beams are more regular and cohesive. In that case, the polarization-enforced ring-structure almost coincides with the region of maximum electric field strength. In contrast, plasma planes generated by an azimuthally polarized beam point in radial direction, extending perpendicularly to the region of maximum field strength.

To perform a more quantitative analysis of the ionization patterns in Fig. 8, we transformed the data of Fig. 8(a) and (c) into a radial coordinate system and took directional averages in both radial and azimuthal directions (Fig. 9(a),(c)). For the azimuthally polarized beam, the radial averages exhibit a strong periodic modulation in azimuthal direction. In the case of the radially polarized beam, the modulation is weak and high carrier densities above half the maximum are present across the whole ring structure. The azimuthal averages show the finite size of the plasma structure, which is determined by the finite beam size for both polarization conditions. Figs. 9(b) and (d) show respective fourier transforms. Only in the case of the azimuthally polarized beam (Fig. 9(b)) a distinct periodicity of about  $500\text{nm}$  in azimuthal direction can be identified in the radial average (green line).

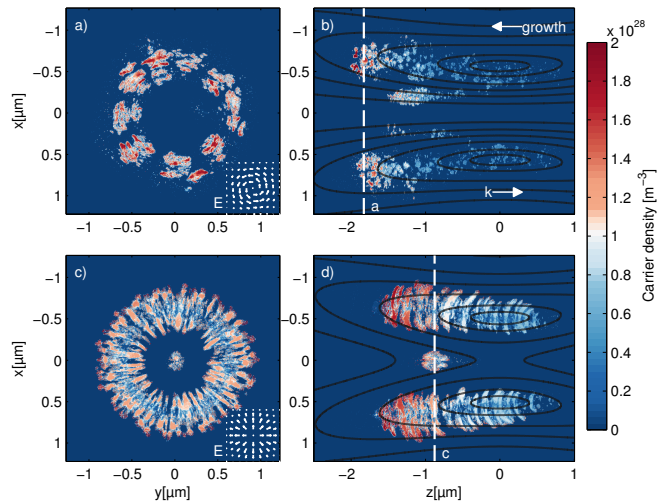


Figure 8: (color online). Carrier density inside a volume filled with inhomogeneities ( $p_{inh} = 0.01$ ) and irradiated with beams with local polarization structure (maximum field strength in the homogeneous case  $E_0 = 1.7 \times 10^{10} \text{Vm}^{-1}$ ,  $NA = 0.5$ ) propagating in  $z$ -direction. a) and b): Azimuthally polarized beam,  $\sigma_{6,inh} = 60\sigma_6$ . c) and d): Radially polarized beam,  $\sigma_{6,inh} = 30\sigma_6$ . Lines of equal field strength  $|E|^2$  as expected in the linear case are overlaid on panels b) and d).

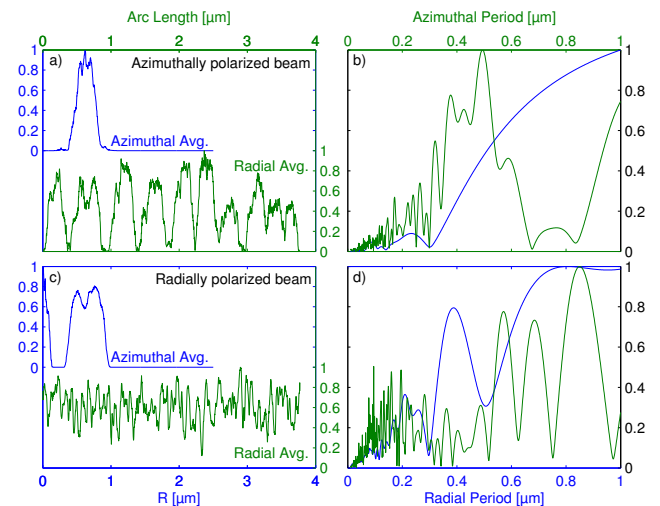


Figure 9: (color online). Structural analysis of the data in Fig.8. a): Directional averages in both azimuthal and radial directions of the data in Fig. 8(a). b): Fourier transforms of the data in a) plotted for structure periods below  $1\mu\text{m}$ . c): Directional averages of the data in Fig. 8(c). d): Fourier transforms of the data in c) plotted for structure periods below  $1\mu\text{m}$ . To obtain the directional averages, the image data has been transformed to a radial coordinate system and averaged over each axis. The radial averages are plotted over the arc length  $l = \theta R_{structure}$  for a nominal structure radius of  $R_{structure} = 600\text{nm}$ .

### III. RELATION TO EXPERIMENTAL RESULTS

In the simulations of our model systems with randomly distributed inhomogeneities, we note strong similarities to experimentally observed volume nanogratings both for beams with spatially homogeneous polarization<sup>30</sup> and beams with a local polarization structure.<sup>6</sup>

Our physical model describes localized ionization and the subsequent growth of nanoplasma, while neglecting the hydrodynamic behaviour of the generated plasma. It thus corresponds to the “nanoplasmonic” model of grating formation suggested in publications by Hnatovski et al.<sup>12</sup>. Contrary to the hypothesis presented there, we do not observe any growth of extended plasma structures for dielectric plasma densities. However close to and above the resonant plasma density where  $\varepsilon_{\text{plasma}} = -2\varepsilon_{\text{background}}$  we do observe the stimulated growth of ionized regions. Although the structures initially grow into the polarization direction, they later organize into thick planes with an orientation orthogonal to the incident electric field.

Despite these similarities with experimental observations our results can only be regarded as a first attempt to understand the laser induced formation of volume gratings in bulk glasses. Due to numerical complexity of the subject we had to simplify the model considerably. Up to now we did not model the evolution of the material in the excited region after the pulse. In fact, real nanogratings form only over the course of many laser pulses. Between individual pulses, the conduction band carriers recombine completely, leaving only chemical and mechanical material modifications as a feedback mechanism for further pulses.<sup>22,24,25</sup> Self-organization emerges as a cumulative effect, and therefore quite likely requires much lower ionization rates.

In our model systems, inhomogeneities are strongly enhanced, allowing for faster ionization of the material. Thus, the purely optical aspects of self-organization can be studied in the course of a single irradiation cycle. Due to its dependence on polarization and wavelength, nanograting formation must be expected to be dominated by optical processes. Consequently, our model should be able to capture some of the essential physics involved. Indeed, self-organization of planes with the correct orientation and a wavelength-related period is reproduced. In the case of an inhomogeneous half-space under planewave irradiation, the commonly observed nanograting period of  $\frac{\lambda}{2n}$  is matched by the simulated plasma structures.

While most publications focussing on high pulse numbers and fully formed gratings report on thin planes with a period of  $\frac{\lambda}{2n}$ , also larger periods around  $\frac{\lambda}{n}$ <sup>31</sup> as well as much thicker grating planes<sup>32</sup> have been observed in experiments with low pulse numbers. Since our model does not include the material modification between pulses, it is not surprising that we observe similar features in the majority of our simulations.

Our results further reproduce the large size as well as the increase in self-organization along the negative z-axis of nanogratings.<sup>32</sup> Both observations can be explained by the backward growth of plasma structures, which is driven by nearfield enhancement and continues well out of the focal region. Experiments have shown, that a similar growth takes place over the course of multiple laser pulses during the generation of nanogratings.<sup>31</sup>

### IV. CONCLUSION

We have modelled the interaction of light with nanoscale inhomogeneities in dielectrics undergoing multiphoton ionization. We observed, that nanoscale inhomogeneities as e.g. voids influence the plasma formation considerably. They induce the formation of large-scale plasma structures with a final shape independent of the initial void. In case of randomly distributed inhomogeneities we observe a strong interaction and subsequent self-organization of evolving plasma structures reproducing some of the key features of nanograting damage patterns in glass.

Further research will include additional ionization mechanisms and a more detailed description of the free carrier dynamics including carrier heating, density and temperature dependent changes of the collision frequency and hydrodynamic phenomena. To fully understand the phenomenon of nanograting-formation, detailed simulations of the material modifications taking place between pulses are required.

### Acknowledgments

The authors gratefully acknowledge financial support by Deutsche Forschungsgemeinschaft (priority program 1327: PE523/-2 and NO462/5-2) and the International Max Planck Research School Physics of Light.

<sup>1</sup> G. Mainfray and G. Manus, Rep. Prog. Phys. **54**, 1333 (1991), URL <http://stacks.iop.org/0034-4885/54/i=10/a=002>.

<sup>2</sup> K. M. Davis, K. Miura, N. Sugimoto, and K. Hirao, Opt. Lett. **21**, 1729 (1996), URL <http://ol.osa.org/abstract.cfm?URI=ol-21-21-1729>.

<sup>3</sup> E. N. Glezer and E. Mazur, Appl. Phys. Lett. **71**, 882

(1997), URL <http://link.aip.org/link/?APL/71/882/1>.

<sup>4</sup> Y. Shimotsuma, K. Hirao, J. Qiu, and P. G. Kazan-sky, Mod. Phys. Lett. B **19**, 225 (2005), URL <http://eprints.soton.ac.uk/20999/>.

<sup>5</sup> V. R. Bhardwaj, E. Simova, P. P. Rajeev, C. Hnatovski, R. S. Taylor, D. M. Rayner, and P. B. Corkum, Phys. Rev. Lett. **96**, 057404 (2006), URL

- <http://link.aps.org/doi/10.1103/PhysRevLett.96.057404>.<sup>21</sup>
- <sup>6</sup> C. Hnatovsky, V. Shvedov, W. Krolikowski, and A. Rode, *Phys. Rev. Lett.* **106**, 123901 (2011), URL <http://link.aps.org/doi/10.1103/PhysRevLett.106.123901>.
  - <sup>7</sup> G. M. Petrov and J. Davis, *J. Phys. B: At., Mol. Opt. Phys.* **41**, 025601 (2008), URL <http://stacks.iop.org/0953-4075/41/i=2/a=025601>.
  - <sup>8</sup> A. Bourgeade, C. Miñócel, and O. Saut, *J. Sci. Comput.* **44**, 170 (2010), ISSN 0885-7474, URL <http://dx.doi.org/10.1007/s10915-010-9375-0>.
  - <sup>9</sup> N. M. Bulgakova, V. P. Zhukov, and Y. P. Meshcheryakov, *Appl. Phys. B* pp. 1–13 (2013), ISSN 0946-2171, URL <http://dx.doi.org/10.1007/s00340-013-5488-0>.
  - <sup>10</sup> C. Mezel, L. Hallo, A. Bourgeade, D. Hebert, V. T. Tikhonchuk, B. Chimier, B. Nkongwa, G. Schurtz, and G. Travaille, *Phys. Plasmas* **15**, 093504 (pages 10) (2008), URL <http://link.aip.org/link/?PHP/15/093504/1>.
  - <sup>11</sup> R. H. Doremus, *J. Am. Ceram. Soc.* **49**, 461 (1966), ISSN 1551-2916, URL <http://dx.doi.org/10.1111/j.1151-2916.1966.tb13299.x>.
  - <sup>12</sup> P. P. Rajeev, M. Gertsvolf, C. Hnatovsky, E. Simova, R. S. Taylor, P. B. Corkum, D. M. Rayner, and V. R. Bhardwaj, *J. Phys. B: At., Mol. Opt. Phys.* **40**, S273 (2007), URL <http://stacks.iop.org/0953-4075/40/i=11/a=S03>.
  - <sup>13</sup> E. S. Efimenko and A. V. Kim, *Phys. Rev. E* **84**, 036408 (2011), URL <http://link.aps.org/doi/10.1103/PhysRevE.84.036408>.
  - <sup>14</sup> E. S. Efimenko, A. V. Kim, and M. Quiroga-Teixeiro, *Phys. Rev. Lett.* **102**, 015002 (2009), URL <http://link.aps.org/doi/10.1103/PhysRevLett.102.015002>.
  - <sup>15</sup> J. R. Peñano, P. Sprangle, B. Hafizi, W. Manheimer, and A. Zigler, *Phys. Rev. E* **72**, 036412 (2005), URL <http://link.aps.org/doi/10.1103/PhysRevE.72.036412>.
  - <sup>16</sup> K. S. Yee, *IEEE Trans. Antennas and Propagation* pp. 302–307 (1966).
  - <sup>17</sup> A. Taflov and S. C. Hagness, *Computational Electrodynamics: The Finite-Difference Time-Domain Method, Third Edition* (Artech House, 2005), 3rd ed., ISBN 1580538320, URL <http://www.worldcat.org/isbn/1580538320>.
  - <sup>18</sup> E. G. Gamaly, S. Juodkazis, K. Nishimura, H. Misawa, B. Luther-Davies, L. Hallo, P. Nicolai, and V. T. Tikhonchuk, *Phys. Rev. B* **73**, 214101 (2006), URL <http://link.aps.org/doi/10.1103/PhysRevB.73.214101>.
  - <sup>19</sup> L. Sudrie, A. Couairon, M. Franco, B. Lamouroux, B. Prade, S. Tzortzakis, and A. Mysyrowicz, *Phys. Rev. Lett.* **89**, 186601 (2002), URL <http://link.aps.org/doi/10.1103/PhysRevLett.89.186601>.
  - <sup>20</sup> X. Mao, S. S. Mao, and R. E. Russo, *Appl. Phys. Lett.* **82**, 697 (2003), URL <http://link.aip.org/link/?APL/82/697/1>.
  - P. Audebert, P. Daguzan, A. Dos Santos, J. C. Gauthier, J. P. Geindre, S. Guizard, G. Hamoniaux, K. Krastev, P. Martin, G. Petite, et al., *Phys. Rev. Lett.* **73**, 1990 (1994), URL <http://link.aps.org/doi/10.1103/PhysRevLett.73.1990>.
  - <sup>22</sup> S. Richter, F. Jia, M. Heinrich, S. Döring, U. Peschel, A. Tünnermann, and S. Nolte, *Opt. Lett.* **37**, 482 (2012), URL <http://ol.osa.org/abstract.cfm?URI=ol-37-4-482>.
  - <sup>23</sup> M. Hasegawa, M. Saneyasu, M. Tabata, Z. Tang, Y. Nagai, T. Chiba, and Y. Ito, *Nuclear Instruments and Methods in Physics Research Section B: Beam Interactions with Materials and Atoms* **166-167**, 431 (2000), ISSN 0168583X, URL <http://linkinghub.elsevier.com/retrieve/pii/S0168583X99010269>.
  - <sup>24</sup> P. P. Rajeev, M. Gertsvolf, E. Simova, C. Hnatovsky, R. S. Taylor, V. R. Bhardwaj, D. M. Rayner, and P. B. Corkum, *Phys. Rev. Lett.* **97**, 253001 (2006), URL <http://link.aps.org/doi/10.1103/PhysRevLett.97.253001>.
  - <sup>25</sup> M. Lancry, B. Poumellec, K. Cook, and J. Canning, in *Proceedings of the International Quantum Electronics Conference and Conference on Lasers and Electro-Optics Pacific Rim 2011* (Optical Society of America, 2011), p. C229, URL <http://www.opticsinfobase.org/abstract.cfm?URI=CLEOPR-2011-C>.
  - <sup>26</sup> C. F. Bohren and D. R. Huffman, *Absorption and scattering of light by small particles*, vol. 1 (Wiley, 1983), URL <http://adsabs.harvard.edu/abs/1983uaz...rept....B>.
  - <sup>27</sup> J. D. Jackson, *Classical electrodynamics* (Wiley, New York, NY, 1999), 3rd ed., ISBN 9780471309321, URL <http://cdsweb.cern.ch/record/490457>.
  - <sup>28</sup> J. E. Sipe, J. F. Young, J. S. Preston, and H. M. van Driel, *Phys. Rev. B* **27**, 1141 (1983), URL <http://link.aps.org/doi/10.1103/PhysRevB.27.1141>.
  - <sup>29</sup> J. Z. P. Skolski, G. R. B. E. Römer, J. V. Obona, V. Ocelik, A. J. Huis in 't Veld, and J. T. M. De Hosson, *Phys. Rev. B* **85**, 075320 (2012), URL <http://link.aps.org/doi/10.1103/PhysRevB.85.075320>.
  - <sup>30</sup> S. Richter, M. Heinrich, S. Döring, A. Tünnermann, and S. Nolte, *Appl. Phys. A: Mater. Sci. Process.* **104**, 503 (2011), ISSN 0947-8396, 10.1007/s00339-011-6489-7, URL <http://dx.doi.org/10.1007/s00339-011-6489-7>.
  - <sup>31</sup> K. Mishchik, G. Cheng, G. Huo, I. M. Burakov, C. Maudclair, a. Mermillod-Blondin, a. Rosenfeld, Y. Ouerdane, a. Boukenter, O. Parriaux, et al., *Optics express* **18**, 24809 (2010), ISSN 1094-4087, URL <http://www.ncbi.nlm.nih.gov/pubmed/21164827>.
  - <sup>32</sup> R. Taylor, C. Hnatovsky, and E. Simova, *Laser & Photonics Review* **2**, 26 (2008), ISSN 18638880, URL <http://doi.wiley.com/10.1002/lpor.200710031>.